frontiers | Frontiers in Physics

TYPE Original Research
PUBLISHED 16 February 2023
DOI 10.3389/fphy.2022.1091325

OPEN ACCESS

EDITED BY
Judith Helena Ojeda Silva,
Universidad Pedagógica y Tecnológica de Colombia, Colombia

REVIEWED BY
Francisco Munoz,
University of Chile, Chile
Ke-Qiu Chen,
Hunan University, China

*CORRESPONDENCE
L. Rosales,
luis.rosalesa@usm.cl

SPECIALTY SECTION
This article was submitted to Condensed Matter Physics, a section of the journal Frontiers in Physics

RECEIVED 06 November 2022
ACCEPTED 23 December 2022
PUBLISHED 16 February 2023

CITATION
González KA, Núñez CD, Orellana PA and Rosales L (2023), Tuning the thermoelectric properties of doped silicene nanoribbon heterostructures. *Front. Phys.* 10:1091325.
doi: 10.3389/fphy.2022.1091325

Tuning the thermoelectric properties of doped silicene nanoribbon heterostructures

K. A. González, C. D. Núñez, P. A. Orellana and L. Rosales*

Departamento de Física, Universidad Técnica Federico Santa María, Valparaíso, Chile

In this work, we investigate the thermoelectrical properties of a silicene nanoribbon heterostructure composed of a central conductor fully doped with ad-atoms and connected to two pristine leads of the same material. Using a tight-binding Hamiltonian, we have calculated the system's thermoelectric properties as a function of the geometrical confinement and external field. Our results exhibit an enhancement of the thermopower when a transverse electric field is applied to the conductor region for different temperatures. In addition, a violation of the Wiedemann–Franz law is observed around the ad-atom energy. Our results suggest the thermoelectric properties of doped silicene nanoribbons can be efficiently tuned with external perturbations.

KEYWORDS

silicene nanoribbons, thermoelectric, Seebeck coefficient, conductance, tight-binding

1 Introduction

In thermal devices, the capacity to transform heat into electricity and *vice versa* is characterized by the thermoelectric efficiency, which is usually described in terms of the dimensionless quantity $ZT = S^2GT/\kappa$ called the figure of merit [1]. In this definition, S is the thermopower or Seebeck coefficient, G is the electronic conductance, and κ is thermal conductance at a temperature T, respectively. It is well known that in a thermoelectric system, both electrons and phonons contribute to heat current. Then, the thermal conductance can be written as $\kappa = \kappa_{el}+\kappa_{ph}$ when the electron–phonon coupling is weak. To obtain an enhanced thermoelectric efficiency, it is necessary to simultaneously reduce both contributions to the thermal conductance without affecting electronic conduction. It cannot be obtained in bulk metallic materials due to the classical Wiedemann–Franz law, which establishes that the ratio $\sigma T/\kappa_{el}$ is a universal constant. Thus, a possible route to improve the thermoelectric materials could be a controlled reduction of the lattice thermal conductance κ_{ph} by increasing phonon scattering [2]. In the last few years, several works have provided theoretical [3–6] and experimental evidence [7–11] that nanostructuring yields thermoelectric efficiency unachievable with bulk materials. In these nanometer systems, the thermal and electronic properties can be tuned independently to achieve improved efficiency above the classical limit. In the literature, ZT values greater than 2.4 have been reported in tailored nanostructured materials such as superlattices [7], nanowires [9], quantum dots [8], or in weak-coupling molecular junctions with electrode doping [12]. Therefore, in this context, nanostructures made of silicene sheets and silicene nanoribbons seem to be good candidates to exhibit high thermoelectric efficiencies [13,14]. Bulk silicene exhibits an in-plane thermal conductivity of 20 W/mK at room temperature, according to equilibrium molecular dynamics simulations [15]. This value is one order of magnitude lower than that of silicon. Silicene has a honeycomb lattice structure, but due to the large ionic radius of silicon atoms, buckling of the lattice is induced [16,17]. Buckling impacts the vibrational modes of

10.3389/fphy.2022.1091325

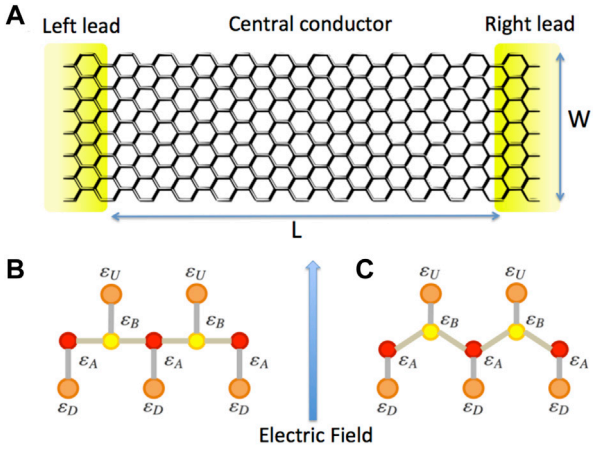

FIGURE 1
(A) Schematic view of the considered ASNR, **(B)** and **(C)** side view of the planar ($\alpha = 0$) and the non-planar ($\alpha \neq 0$) Silicene nanostructures. In this panel, $\varepsilon_{(U,D)}$ represents the on-site energy of the ad-atoms pinned at the A(B) ribbon sites.

silicene, reducing phonon heat conduction. Finally, the quantum effects allow thermoelectric devices to overcome the limitations to the classical Wiedemann–Franz law. Nanodevices with sharp resonances in electron transmission (such as Fano lineshapes) are good candidates for highly efficient heat-to-electricity converters because the ratio GT/κ_{el} increases well above the classical Wiedemann–Franz limit [18–24].

In this context, we have studied the thermoelectric properties of the doped silicene nanoribbon heterostructure as a function of the geometrical confinement and the presence of an external electric field. Considering a central conductor region fully doped with ad-atoms and connected to two pristine leads, we calculated the electronic conductance, the Seebeck coefficient, the electronic thermal conductance, the Lorenz number, and the electronic figure of merit of armchair silicene nanoribbons. We have found an enhancement of the thermopower of the device at different temperatures when a transverse electric field is applied to the conductor region. Consequently, we have obtained great values of ZT_{el} as the external potential is increased for different temperatures. Finally, we have obtained a violation of the Wiedemann–Franz law for different external potential intensities and temperatures. Our results suggest that with an appropriate gate configuration, the thermoelectric properties of doped silicene nanoribbons can be efficiently tuned.

2 Model and formalism

The system under the study consists of a fully doped rectangular silicene nanoribbon (SNR) of width W and length L connected to source and drain leads made of pristine SNRs, as shown schematically in Figure 1. To avoid topologically protected edge states that appear at the Fermi energy in zig-zag nanoribbons, we restrict ourselves to nanoribbons with armchair edges (A-SNR) hereafter. Electronic properties in these ribbons have been described by using a single-band tight-binding approximation [25]. For this purpose, the system is split into three spatial regions: left contact, scattering region (conductor), and right contact. The Hamiltonian of the doped A-SNR ribbon can be written in the single-band tight-binding scheme as follows:

$$H_T = \sum_{i=1}^{N} \varepsilon_i c_i^{\dagger} c_i + \gamma \sum_{i,j}^{N} \left(c_i^{\dagger} c_j + h.c \right), \tag{1}$$

where $c_i\,(c_i^{\dagger})$ are the annihilation (creation) electronic operators, γ is the hopping coupling between the nearest neighbor atoms (we have considered $\gamma \sim 1.0$ eV), and ε_i is the on-site energy of the *ith* A(B) atom of the ribbon. For simplicity, we have fixed the on-site energy of the right and left leads at $\varepsilon_i = 0$. In our model, we have re-normalized the energy of each A(B) site of the central conductor in such a way that it contains all the information on the ad-atoms pinned at both sides of the ribbon [Figure 1B)] and the electrostatic potential generated by the applied external electric field. Thus, the on-site energy ε_i for the A(B) atoms of the conductor can be rewritten as

$$\begin{aligned} \varepsilon_i^A &= \alpha U_E + \frac{\Gamma^2}{\varepsilon - \varepsilon_D} \\ \varepsilon_i^B &= -\alpha U_E + \frac{\Gamma^2}{\varepsilon - \varepsilon_U}, \end{aligned} \tag{2}$$

where Γ is the coupling between the ad-atoms and the ribbon's A(B) atoms. $U_E = l\,E$ is the electrostatic potential generated by the electric field E, considering l as the vertical separation between both sub-lattices in the ribbon; therefore, $\varepsilon_{U(D)} = \varepsilon_0 \pm U_E$. We introduce the parameter α as a measure of ribbon buckling so that $0 \leq \alpha \leq 1$. It should be noticed that if the ribbon is planar ($\alpha = 0$), the electrostatic potential affects only the energy of the ad-atoms. Therefore, a differentiation is generated between both sub-lattices of the ribbon. On the other hand, if $\alpha \neq 0$, the electrostatic potential affects both ribbons' sub-lattices (staggered potential) and the ad-atoms. Therefore, this electrostatic potential's effects on the buckled ribbon's electronic properties are stronger than those in the planar case.

To analyze the thermoelectric behavior of the doped A-SNR, we have adopted the linear response approximation, in which an effective voltage drop ΔV and a temperature difference ΔT are applied between the left and right contacts. Within this approach, the electronic current I_e and the heat current I_Q are given by

$$I_e = -e^2 K_0 \Delta V + \frac{e}{T} K_1 \Delta T, , \tag{3}$$

$$I_Q = eK_1 \Delta V - \frac{1}{T} K_2 \Delta T, \tag{4}$$

where e is the electron charge, T is the absolute temperature, and K_n (with $n = 0, 1, 2$) is the thermal integral defined as

$$K_n(\mu, T) = \frac{2}{h} \int_0^{\infty} d\varepsilon\, \mathcal{T}(\varepsilon)\, (\varepsilon - \mu)^n \left(-\frac{\partial f(\varepsilon, T)}{\partial \varepsilon} \right). \tag{5}$$

Here, h is the Planck constant, μ is the chemical potential, $f(\varepsilon, T)$ is the equilibrium Fermi–Dirac distribution, and $\mathcal{T}(\varepsilon)$ is the energy-dependent electron transmission probability.

The electronic conductance is defined as $G = -I_e/\Delta V$, and it can be obtained directly from Equation 3.

$$G(\mu, T) = e^2 K_0. \tag{6}$$

The Seebeck coefficient S is calculated in the linear response regime, namely, $|\Delta T| \ll T$ and $|e\Delta V| \ll \mu$. It is defined as the voltage drop induced by a temperature gradient at zero electric current, $S = \Delta V/\Delta T|_{Ie} = 0$ [Eq. 3], in the limit $\Delta T \to 0$. Thus,

$$S(\mu,T) = -\frac{1}{eT}\frac{K_1}{K_0}. \tag{7}$$

The electron contribution to the thermal conductance is defined as the ratio between the thermal current I_Q and the temperature gradient ΔT when the electric current I_e is zero, $\kappa_{el} = I_Q/\Delta T|_{I_e=0}$. Written in terms of the thermal integrals, it is given by

$$\kappa_{el}(\mu,T) = \frac{1}{T}\left(K_2 - \frac{K_1^2}{K_0}\right). \tag{8}$$

Finally, we have calculated the Lorenz number for the considered heterostructures, which is defined as

$$\mathcal{L} = \frac{\kappa_{el}}{\sigma T}, \tag{9}$$

where σ is the electronic conductivity and T is the temperature of the system. For metals, this relation remains constant, with a value of $\frac{\pi^2}{3}\left(\frac{k_b}{e}\right)^2 = 2,44 \times 10^{-8} V^2 K^{-2}$, where k_b is the Boltzmann constant and e is the electron charge.

We have analytically determined the transmission function of the system as a function of the energy. For this purpose, we have used an effective model in which the nanoribbon is mapped into a one-dimensional diatomic chain (See the Supplementary Material). Thus, the total transmission $\mathcal{T}(\varepsilon)$ is written as

$$\mathcal{T}(\varepsilon) = \frac{R_c (S_{1,1})^2\left[\left(S^c_{N+1,0}\right)^2\mathcal{F}_1 + \left(S^c_{N+2,1}\right)^2\mathcal{F}_2 + 2\left(S^c_{N+2,1}\right)^2\mathcal{F}_3 - 2S^c_{N,-1}\mathcal{F}_4 + \left(S^c_{N,1}\right)^2\right]}{\left(R_c^2 + 1 - 2R_c C^{1,1}_{-1,1}\right)\left[\mathcal{F}_5 + R_c^2\mathcal{F}_6 - 2R_c\mathcal{F}_7 + 2R_c^2\mathcal{F}_8\right]}. \tag{10}$$

Considering $C^{i,j}_{p,q} = \cos[(ik_c - j\theta_c) + (pk - q\theta)]$ and defining $z^c = e^{i[k_c - \theta_c]}$ and $S^c_{p,q} = \sin[pk_c + q\theta_c]$ for the conductor, and $z = e^{i[k-\theta]}$ and $S_{p,q} = \sin[pk + q\theta]$ for each lead, the $\mathcal{F}_i$ functions are defined by

$$\begin{aligned}
\mathcal{F}_1 &= \left(R_c^2 + 1\right) + 2R_c C^{1,1}_{1,1},\\
\mathcal{F}_2 &= R_c^2\left[1 - 2S^c_{N+1,9}C^{1,1}_{0,0}\right],\\
\mathcal{F}_3 &= R_c\left[S^c_{N,1}C^{1,1}_{-1,1} - S^c_{N+1,0}C^{0,0}_{1,1}\right],\\
\mathcal{F}_4 &= S^c_{N+1,0}\left[R_c C^{0,0}_{1,1} + C^{1,1}_{0,0}\right],\\
\mathcal{F}_5 &= \left(R_c^2 + 1\right)^2\left(S^c_{N+1,0}\right)^2,\\
\mathcal{F}_6 &= \left(S^c_{N,1}\right)^2 + \left(S^c_{N+2,-1}\right)^2,\\
\mathcal{F}_7 &= \left(R_c^2 + 1\right)S^c_{N+1,0}C^{0,0}_{1,1}\left[S^c_{N,1} + S^c_{N+2,-1}\right],\\
\mathcal{F}_8 &= S^c_{N,1}S^c_{N+2,-1}\left[\left(C^{0,0}_{1,1}\right)^2 - S_{1,-1}\right].
\end{aligned}$$

In the aforementioned equations, we have considered the following definitions:

$$\begin{aligned}
k &= \arccos\left[\frac{\varepsilon^2 - \gamma^2\left(1 + 4\cos^2 q_m\right)}{4\gamma^2\cos q_m}\right],\\
k_c &= \arccos\left[\frac{(\varepsilon - \varepsilon_A)(\varepsilon - \varepsilon_B) - \gamma^2\left(1 + 4\cos^2 q_m\right)}{4\gamma^2\cos q_m}\right],\\
R_c &= \sqrt{\frac{\varepsilon - \varepsilon_A}{\varepsilon - \varepsilon_B}},\\
\theta &= \arctan\left[\frac{2\cos q_m \sin k}{1 + 2\cos q_m\cos k}\right],\\
\theta_c &= \arctan\left[\frac{2\cos q_m \sin k_c}{1 + 2\cos q_m\cos k_c}\right],
\end{aligned} \tag{11}$$

where k_c and k are the wavenumbers in the effective one-dimensional chain, θ_c and θ are phases between the A(B) atoms in the ribbons, and q_m is the discrete electronic wavenumber obtained by imposing the hard-wall boundary condition to the ribbon width. In armchair nanoribbons $q_m = m\pi/(M+1)$, with $m = 1, 2, \ldots, M$, which corresponds to the number of transverse energy channels available in the ribbon.

3 Results

The results for the transmission function $\mathcal{T}(\varepsilon)$ for an A-SNR of width $N = 5$, conductor length $L = 80$ (measured in unit cells), and $\alpha = 0.1\gamma$ for different potential intensities U are exhibited in Figure 2. We have considered two different ad-atoms' energies: *i*) $\varepsilon_0 = 0\ \gamma$ [panels (a) and (c)] and *ii*) $\varepsilon_0 = 0.1\ \gamma$ [panels (b) and (d)]. These plots exhibit the standard transmission function behavior for a quasi-one-dimensional system, reflecting the number of discrete wavenumbers allowed in the transverse direction of the ribbon. However, centered at the ad-atom energy, an electronic gap becomes larger and noisy as the external potential U is increased. Furthermore, it is possible to observe in Figures 2C, D that there is an asymmetry of the transmission function at the gap edges, especially if the ad-atom energy differs from the on-site energy of the A(B) sub-lattices of the ribbon. As is shown further in this paper, the abrupt changes in $\mathcal{T}(\varepsilon)$ affect the thermoelectrical behavior of the heterostructure. We have analyzed the behavior of the transmission $\mathcal{T}(\varepsilon)$ as a function of α, considering fixed values of the potential U. Due to the form that we have modeled the on-site energy at the conductor region and analyzing how Eqs 10, 11 depend on α, we can affirm that the primary physical mechanism that affects the transmission of electrons through the heterostructure is the external field. In this sense, without loss of generality, hereafter, we will use a realistic value of $\alpha = .1$.

The results for the electronic conductance G and the Seebeck coefficient S for a $N = 5$ A-SNR, of length $L = 80$ and $\alpha = .1$, for different potential intensities U and different temperatures are exhibited in Figure 3 (a) and (c). To analyze the case of an impurity other than a silicon atom of the ribbon, we have chosen the ad-atom energy $\varepsilon_0 = 0.1\ \gamma$. At room temperature ($300K$), it is possible to observe that U strongly affects the behavior of G, progressively generating a conductance gap for U values greater than $0.1\ eV$. It is a consequence of the $\mathcal{T}(\varepsilon)$ behavior for different potentials U shown in Figure 2D. The smoothness of the conductance curves around the ad-atom energy is produced by the Fermi–Dirac distribution at room temperature, which weighs the behavior of the thermal integral K_0 used to define G in Eq. 6. Furthermore, and as is expected, for a fixed value of U, the conductance vs. temperature curve behaves as a standard semiconductor, showing slight variations as the temperature increases, as shown in Figure 3C.

On the other hand, in Figure 3B, we show that the Seebeck coefficient S presents a crescent value of its maximum as the external potential U increases. This behavior is a direct consequence of the noisy and asymmetric curves of transmission $\mathcal{T}(\varepsilon)$ around the ad-atom energy, shown in Figure 2 (d). It is well known that S strongly depends on the behavior of $\mathcal{T}'(\varepsilon) = \partial\mathcal{T}(\varepsilon)/\partial\varepsilon$. Therefore, abrupt changes in the transmission function will produce an enhancement of the thermopower of the system. To better visualize this point, it is useful to examine the Sommerfeld expansion of thermal integrals K_0 and K_1 and then replace them on Eq. 7. It generates a dominant term in the expansion of the Seebeck coefficient of the form $S \approx (\varepsilon - \mu)\mathcal{T}'(\mu)/\mathcal{T}(\mu)$ which defines the shape and the maximum of the thermopower. Thus, the noisier an asymmetric is in the transmission $\mathcal{T}(\varepsilon)$, the higher the Seebeck maximum S_{max} can be obtained. The ratio $\mathcal{T}'(\mu)/\mathcal{T}(\mu)$ is not linear, and it is expected that for

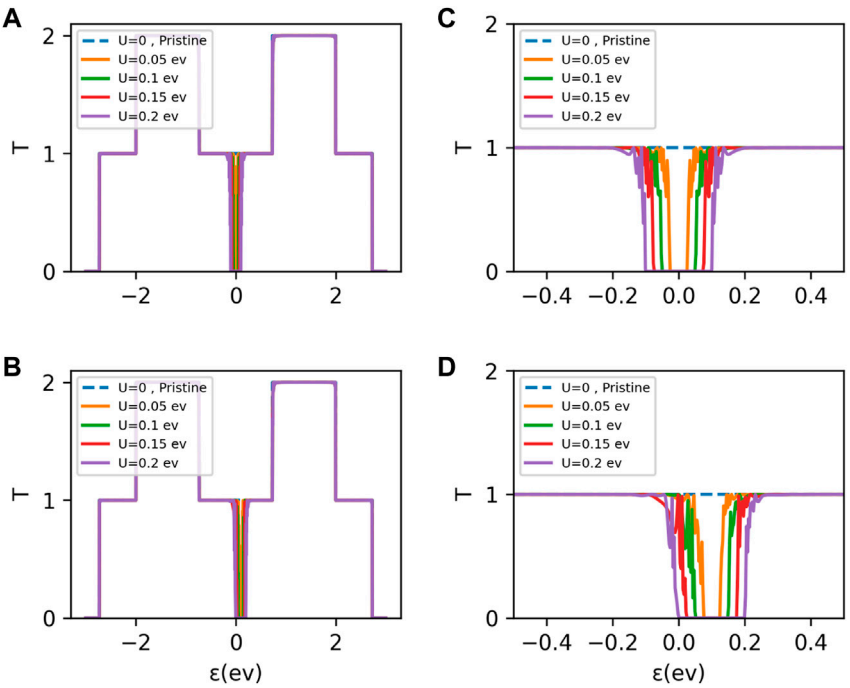

FIGURE 2
Transmission vs. Fermi energy for an A-SNR of width $N = 5$ and length $L = 80$ for several external potential intensities, considering two different on-site energies for the ad-atoms. In **(A)** $\varepsilon_0 = 0$ and **(B)** $\varepsilon_0 = 0.1\gamma$. In both panels, the pristine $N = 5$ A-SNR has been included as references (dashed blue line). Panels **(C)** and **(D)** are zoomed in to the region of interest (around the energy of the ad-atoms). All curves were made considering $\alpha = 0.1$.

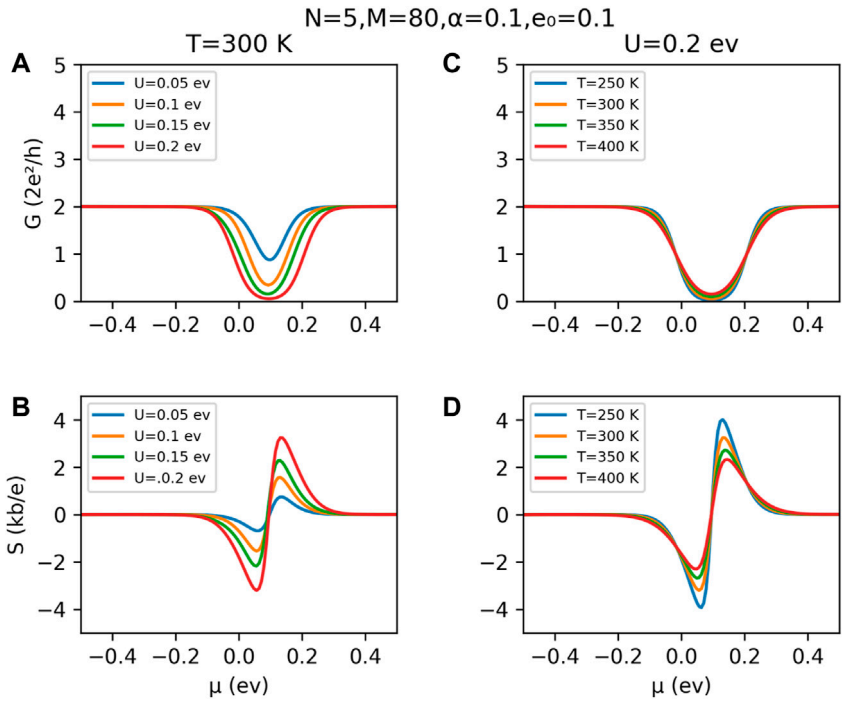

FIGURE 3
Electronic conductance and thermopower for an A-SNR of width $N = 5$ and length $L = 80$. In panels **(A)** and **(B),** we have fixed the temperature in 300K, and then variations of the external potential intensity, whereas in panels **(C)** and **(D),** we have considered variations of the temperature of the heterostructure.

10.3389/fphy.2022.1091325

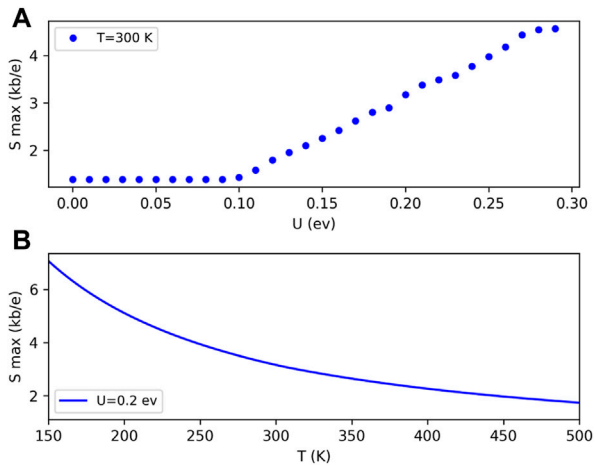

FIGURE 4
Maximum of the Seebeck coefficient behavior (S_{max}) as a function of **(A)** external potential intensity for room temperature and **(B)** temperature, for a fixed external potential U.

specific values of U, the maximum S_{max} tends to saturate. It is what we have obtained, and in the case of $N = 5$ A-SNR, this potential value is around $U \sim 0.25\,eV$, as shown in Figure 4A. It is interesting to mention that in this plot, S_{max} starts to increase for $U \sim 0.1$eV, which corresponds to the on-site energy for the ad-atoms at the conductor region. Just at this energy, the ratio between the thermal integrals K_1 and K_0 defines this behavior. Although the K_0 function opens a gap around the impurity energy, the K_1 function changes its slope around it so that the ratio is maximized as the U potential is increased. The maximum of the Seebeck coefficient decreases as the temperature of the system increases, for the potential intensity fixed (for instance, at $U = 0.2\,eV$), as shown in Figure 3D and Figure 4B. This behavior is mainly because the Fermi–Dirac distribution becomes a smooth energy function as the temperature increases. Therefore, the thermal integrals K_0 and K_1 are weighted by a broad-band energy function, which absorbs any abrupt change in the transmission function $\mathcal{T}(\varepsilon)$.

The results for the electronic conductance, the electronic thermal conductance, and the Lorenz number for a $N = 5$ A-SNR of length $L = 80$ and $\alpha = 0.1$, for different potential intensities U and different temperatures T, are exhibited in Figure 5. In these plots, it is possible to observe that the electronic thermal conductance κ_{el} is affected by the variations of U and T [panels (b) and (e), respectively], reducing its value around the ad-atom energy ($\varepsilon_0 = 0.1\ \gamma$) and generating a gap behavior that differs with respect to the conductance curves [panels (a) and (d)]. The κ_{el} gap becomes broader and softens compared to the G gap. In addition, for different values of the external potential U and temperatures T and just at the ad-atom energy, κ_{el} exhibits an increase from the thermal integrals' behavior K_0, K_1, and K_2 at this energy. Thus, if we considered the Sommerfeld expansion of these integrals, the dominant terms in the definition of κ_{el} will be quadratic in the transmission function derivative and on the energy so that $\kappa_{el} \approx (\varepsilon - \mu)^2 \mathcal{T}'^2(\mu)/\mathcal{T}(\mu)$. Thus, for energies close to the ad-atom energies, κ_{el} shows this small increase that plays an essential role in the thermoelectrical properties of the system.

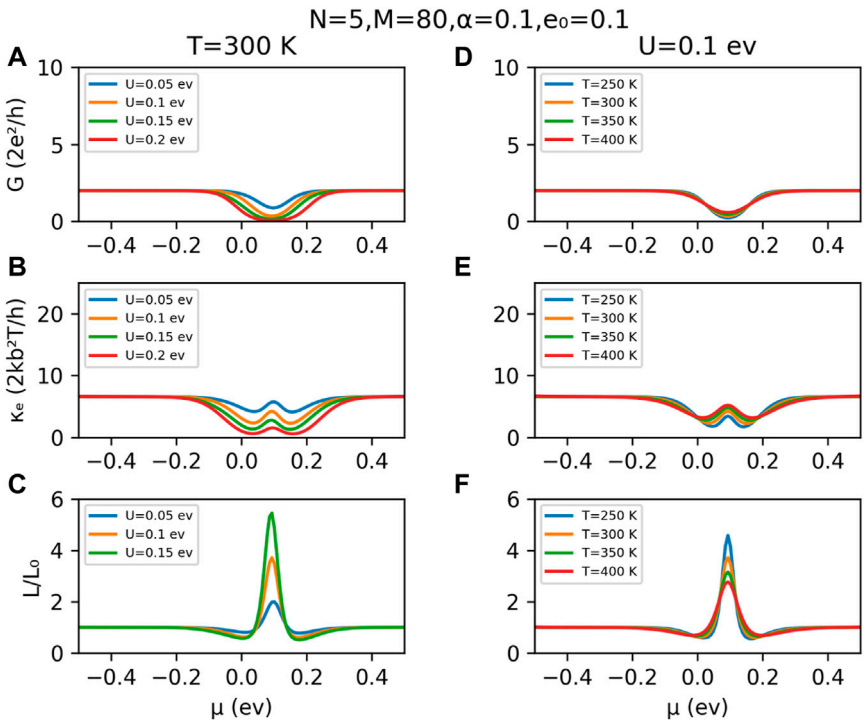

FIGURE 5
Electronic conductance, electronic thermal conductance, and Lorenz number for an A-SNR of width $N = 5$ and length $L = 80$. We have plotted panels **(A)**, **(B),** and **(C)** for room temperature, increasing the external potential intensity. In panels **(D)**, **(E),** and **(F),** we have considered variations of the temperature of the system.

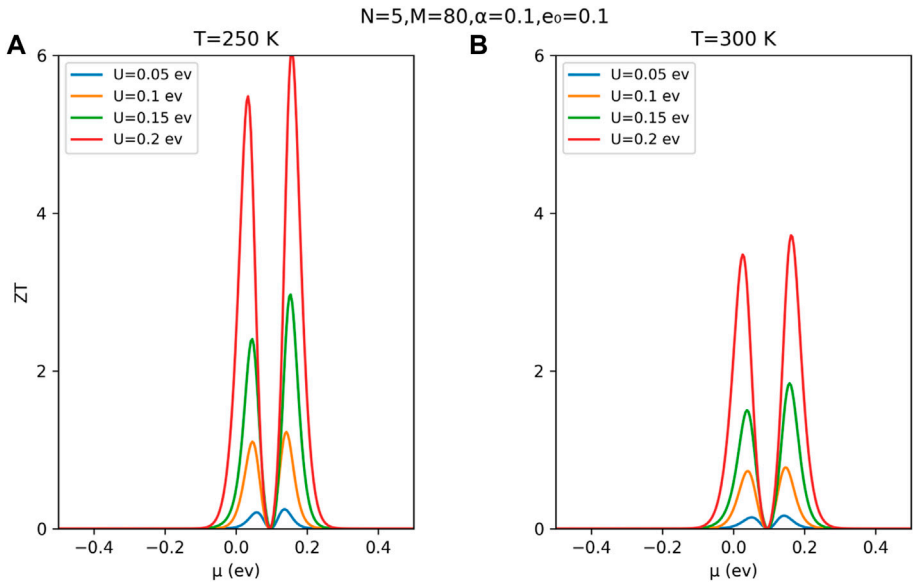

FIGURE 6
Electronic figure of merit as a function of the chemical potential, for an A-SNR of width $N = 5$ and length $L = 80$. We have plotted panels **(A)** and **(B)** for two different temperatures, increasing the external potential intensity.

In this context, by using the definition given in Eq. 9, we have calculated the Lorenz number $\mathcal{L}$ (measured in the unit of $\mathcal{L}_0 = (\pi k_b)^2/3e^2$) for different values of external potential U and different temperatures T, as it is shown in Figures 5C, F. For normal metals, $\mathcal{L}/\mathcal{L}_0 \approx 1$ remains constant as a function of energy or the chemical potential of the system. However, the Lorenz number changes, increasing its value over $\mathcal{L}_0$ just around the impurity energy, for nanostructures that present quantum confinement and interference effects, such as those promoted by the ad-atoms in the central conductor of our heterostructure. It is the so-called violation of the classical Wiedemann–Franz law and represents clear evidence of the presence of quantum phenomena in the system. Thus, it is possible to observe in our case at chemical potential $\mu = 0.1\ eV$, for several values of U and T, that $\mathcal{L}/\mathcal{L}_0$ presents larger values, which tends to decrease as the temperature and the external potential are increased. It is direct to understand the changes in the Lorenz number of the system and the origin of the violation of the Wiedemann–Franz law in our system, observing the ratio between the conductance curves of panels (a) and (d) and the electronic thermal conductance curves of panels (b) and (e).

In order to estimate the thermoelectrical efficiency of the proposed system, we present results for the electronic figure of merit $ZT_{el} = TS^2G/\kappa_{el}$, which are displayed in Figure 6. For these calculations, we have not considered the phonon contribution to the thermal conductance because it is well-known that in narrow pristine A-SNR, $\kappa_{ph} \leq \kappa_{el}$ [*see* Pan et al. [14] for a complete analysis of these quantities]. In this sense, we expect that the ad-atoms in the central conductor would reduce even more the lattice contribution to the total thermal conductance of the system κ. As it is observed in both panels of Figure 6, as the external potential intensity is increased, the thermal efficiency becomes better. In addition, as the temperature is increased, the maximum of ZT_{el} tends to reduce its magnitude. Both results are a direct consequence of the Seebeck coefficient behavior as a function of the external potential and the temperature, as it is shown in Figure 3 and Figure 4. The electronic figure of merit depends quadratically on S; therefore, any abrupt change on this thermal quantity strongly affects the thermoelectrical efficiency of the proposed system.

4 Final remarks

In this work, we have studied the thermoelectrical properties of armchair silicene nanoribbon heterostructures. Using an effective one-dimensional model, we have determined the electron transmission function of the system analytically. With this result, we have calculated and analyzed the behavior of the electronic conductance, the Seebeck coefficient, and the electronic contribution to the thermal conductance as a function of an external potential intensity and the temperature. We have obtained a controlled tuning of the Seebeck coefficient maximum $S_{\max}$ at room temperature as the external potential U is modified. This behavior is explained by the abrupt changes in the transmission function around the electronic gap produced by the ad-atoms. Furthermore, as expected, as the system's temperature increases, $S_{\max}$ decreases because the transmission changes become smooth, especially for temperatures above $300K$.

In the case of electronic thermal conductance, we have obtained a reduction of its magnitude around the ad-atom energy as U increases. However, this reduction is less than that obtained for the electronic conductance at the same energy range. Therefore, we have obtained a violation of the classical Wiedemann–Franz law, reflected in the Lorenz number behavior, which presents a clear dependence on the external potential intensity U and the temperature of the system.

It is important to mention that the obtained thermoelectric efficiency only considers the electronic contribution to the thermal conductance. Independently that we expect a strong reduction to the phonon mean free path due to the presence of the ad-atoms, the lattice contribution to the thermal conductance will not be zero; therefore, the total figure of merit should be less than that of our results but still better in comparison with the pristine case.

The thermoelectric behavior described in this work is quite general for the considered heterostructures. We have obtained similar results for different geometrical configurations, considering variations in the width and length of the conductor region. In this sense, we have focused on the simplest system to give a better physical understanding of the thermoelectrical phenomena present in these nanostructures.

Data availability statement

The raw data supporting the conclusion of this article will be made available by the authors, without undue reservation.

Author contributions

KG and CN performed the analytic and numerical calculation. PO and LR conceived the study. All authors wrote and contributed to the final version of the manuscript and approved the submission.

Funding

This work was financially supported by FONDECYT (grant numbers: 1220700 and 1201876).

Conflict of interest

The authors declare that the research was conducted in the absence of any commercial or financial relationships that could be construed as a potential conflict of interest.

Publisher's note

Supplementary material

Supplementary Material for this article can be found online at: https://www.frontiersin.org/articles/10.3389/fphy.2022.1091325/full#supplementary-material

References

1. Goldsmid HJ. *Introduction to thermoelectricity*. Berlin: Springer (2010).

2. Gayner C, Kar KK. Recent advances in thermoelectric materials. *Prog Mater Sci* (2016) 83:330–82. doi:10.1016/j.pmatsci.2016.07.002

3. Hicks LD, Dresselhaus MS. Thermoelectric figure of merit of a one-dimensional conductor. *Phys Rev B* (1993) 47:16631–4. doi:10.1103/physrevb.47.16631

4. Khitun A, Balandin A, Liu JL, Wang KL. In-plane lattice thermal conductivity of a quantum-dot superlattice. *J Appl Phys* (2000) 88:696–9. doi:10.1063/1.373723

5. Balandin AA, Lazarenkova OL. Mechanism for thermoelectric figure-of-merit enhancement in regimented quantum dot superlattices. *Appl Phys Lett* (2003) 82: 415–7. doi:10.1063/1.1539905

6. Sadeghi H, Sangtarash S, Lambert CJ. Enhancing the thermoelectric figure of merit in engineered graphene nanoribbons. *Beilstein J Nanotechnol* (2015) 6:1176–82. doi:10.3762/bjnano.6.119

7. Venkatasubramanian R, Siivola E, Colpitts T, O'Quinn B. Thin-film thermoelectric devices with high room-temperature figures of merit. *Nature (London)* (2001) 413: 597–602. doi:10.1038/35098012

8. Harman TC, Taylor PJ, Walsh MP, LaForge BE. Quantum dot superlattice thermoelectric materials and devices. *Science* (2002) 297:2229–32. doi:10.1126/science.1072886

9. Hochbaum AI, Chen R, Delgado RD, Liang W, Garnett EC, Najarian M, et al. Enhanced thermoelectric performance of rough silicon nanowires. *Nature (London)* (2008) 451:163–7. doi:10.1038/nature06381

10. Boukai AI, Bunimovich Y, Tahir-Kheli J, Yu J-K, Goddard WA, Heath JR. Silicon nanowires as efficient thermoelectric materials. *Nature (London)* (2008) 451:168–71. doi:10.1038/nature06458

11. Chen X-K, Chen K-Q. Thermal transport of carbon nanomaterials. *J Phys Condensed Matter* (2020) 32:153002. doi:10.1088/1361-648x/ab5e57

12. Wu D, Cao X, Jia P, Zeng YJ, Feng YX, Tang LM, et al. Excellent thermoelectric performance in weak coupling molecular junctions with electrode doping and electrochemical gating. *Sci China Phys Mech Astron* (2020) 63:276811. doi:10.1007/s11433-019-1528-y

13. Zberecki K, Wierzbicki M, Barnaś J, Swirkowicz R. Thermoelectric effects in silicene nanoribbons. *Phys Rev B* (2013) 88:115404. doi:10.1103/physrevb.88.115404

14. Pan L, Liu HJ, Tan XJ, Lv HY, Shi J, Tang XF, et al. Thermoelectric properties of armchair and zigzag silicene nanoribbons. *Phys Chem Chem Phys* (2012) 14:13588–93. doi:10.1039/C2CP42645E

15. Li H-P, Zhang R. Vacancy-defect–induced diminution of thermal conductivity in silicene. *EPL (Europhys. Lett.)* (2012) 99:36001. doi:10.1209/0295-5075/99/36001

16. Aufray B, Kara A, Vizzini S, Oughaddou H, Léandri C, Ealet B, et al. Graphene-like silicon nanoribbons on ag(110): A possible formation of silicene. *Appl Phys Lett* (2010) 96: 183102. doi:10.1063/1.3419932

17. Lalmi B, Oughaddou H, Enriquez H, Kara A, Vizzini S, Ealet B, et al. Epitaxial growth of a silicene sheet. *Appl Phys Lett* (2010) 97:223109. doi:10.1063/1.3524215

18. Mahan GD, Sofo JO. The best thermoelectric. *Proc Natl Acad Sci USA* (1996) 93: 7436–9. doi:10.1073/pnas.93.15.7436

19. Gómez-Silva G, Ávalos-Ovando O, Ladrón de Guevara ML, Orellana PA. Enhancement of thermoelectric efficiency and violation of the Wiedemann-Franz law due to Fano effect. *J Appl Phys* (2012) 111:053704. doi:10.1063/1.3689817

20. Zheng J, Zhu M-J, Chi F. Fano effect on the thermoelectric efficiency in parallel-coupled double quantum dots. *J Low Temp Phys* (2012) 166:208–17. doi:10.1007/s10909-011-0417-2

21. García-Suárez VM, Ferradás R, Ferrer J. Impact of Fano and Breit-Wigner resonances in the thermoelectric properties of nanoscale junctions. *Phys Rev B* (2013) 88:235417. doi:10.1103/physrevb.88.235417

22. Fu H-H, Gu L, Wu D-D, Zhang Z-Q. Enhancement of the thermoelectric figure of merit in DNA-like systems induced by Fano and Dicke effects. *Phys Chem Chem Phys* (2015) 17:11077–87. doi:10.1039/c4cp04382k

23. Sierra MA, Saiz-Bretín M, Domínguez-Adame F, Sánchez D. Interactions and thermoelectric effects in a parallel-coupled double quantum dot. *Phys Rev B* (2016) 93: 235452. doi:10.1103/physrevb.93.235452

24. Wang R-N, Dong G-Y, Wang S-F, Fu G-S, Wang J-L. Impact of contact couplings on thermoelectric properties of anti, Fano, and Breit-Wigner resonant junctions. *J Appl Phys* (2016) 120:184303. doi:10.1063/1.4967751

25. Ezawa M. A topological insulator and helical zero mode in silicene under an inhomogeneous electric field. *New J Phys* (2012) 14:033003. doi:10.1088/1367-2630/14/3/033003